J Toxicol Pathol 2018; 31: 293–300

Original Article

Difference in morphology and interactome profiles between orthotopic and subcutaneous gastric cancer xenograft models

Kiyotaka Nakano[1*†], Takashi Nishizawa[1†], Daisuke Komura[2], Etsuko Fujii[1, 3], Makoto Monnai[4], Atsuhiko Kato[3], Shin-ichi Funahashi[1], Shumpei Ishikawa[2], and Masami Suzuki[1*]

[1] Forerunner Pharma Research Co., Ltd., Komaba Open Laboratory, The University of Tokyo, 4-6-1 Komaba, Meguro-ku, Tokyo 153-8904, Japan
[2] Department of Genomic Pathology, Medical Research Institute, Tokyo Medical and Dental University, Tokyo 113-8510, Japan
[3] Chugai Pharmaceutical Co., Ltd., 200 Kajiwara, Kamakura, Kanagawa 247-8530, Japan
[4] Chugai Research Institute for Medical Science Co., Ltd., 200 Kajiwara, Kamakura, Kanagawa 247-8530, Japan

Abstract: In xenograft models, orthotopic (ORT) engraftment is thought to provide a different tumor microenvironment compared with subcutaneous (SC) engraftment. We attempted to characterize the biological difference between OE19 (adenocarcinoma of the gastroesophageal junction) SC and ORT models by pathological analysis and CASTIN (CAncer-STromal INteractome) analysis, which is a novel method developed to analyze the tumor-stroma interactome framework. In SC models, SCID mice were inoculated subcutaneously with OE19 cells, and tumor tissues were sampled at 3 weeks. In ORT models, SCID mice were inoculated under the serosal membrane of the stomach wall, and tumor tissues were sampled at 3 and 6 weeks after engraftment. Results from the two models were then compared. Histopathologically, the SC tumors were well circumscribed from the adjacent tissue, with scant stroma and the formation of large ductal structures. In contrast, the ORT tumors were less circumscribed, with small ductal structures invading into abundant stroma. Then we compared the transcriptome profiles of human tumor cells with the mouse stromal cells of each model by species-specific RNA sequencing. With CASTIN analysis, we successfully identified several interactions that are known to affect the tumor microenvironment as being selectively enhanced in the ORT model. In conclusion, pathological analysis and CASTIN analysis revealed that ORT models of OE19 cells have a more invasive character and enhanced interaction with stromal cells compared with SC models. (DOI: 10.1293/tox.2018-0020; J Toxicol Pathol 2018; 31: 293–300)

Key words: ubcutaneous, orthotopic, CASTIN, interactome, microenvironment

Introduction

Cancer xenograft models are widely used to study tumorigenesis or to examine response to therapy. Xenograft models are classified as subcutaneous (SC) or orthotopic (ORT), and researchers select models according to the objective of a study. SC models are often used to assess antitumor activity because of their high reproducibility and ease of monitoring cancer growth. On the other hand, ORT models are thought to reproduce some aspects of the cancer microenvironment and are thought to be more clinically relevant than SC models[1–5]. ORT models emulate a number of important biological features of cancer progression[6, 7], metastasis[8–10], and sensitivity to therapy[11–13]. These differences between models might be associated with a difference in the cancer microenvironment, but detailed mechanisms are still unclear.

We previously reported CASTIN (CAncer-STromal INteractome) analysis, a novel framework that evaluates the cancer-stromal interactome[14] and can be used to understand the relationship between a cancer and its microenvironment. As there is an approximately 15% sequence difference between human and mouse exon sequences[15], a simultaneous transcriptome analysis of cancer and stroma can be achieved using RNA sequencing data from xenografts[16]. CASTIN summarizes the interactome status between cancer and stroma by quantitatively evaluating the ligand-receptor expression and comprehensively visualizing that expression to identify critical cancer microenvironment interactions. In a previous report, CASTIN was applied to a data set from pancreas ductal adenocarcinoma, and that individual cancer was successfully characterized in terms of its cancer-stroma relationships[14].

Received: 5 April 2018, Accepted: 22 July 2018
Published online in J-STAGE: 13 August 2018
*Corresponding authors: K Nakano
(e-mail: nakanokyt@chugai-pharm.co.jp)
M Suzuki (e-mail: suzukimsm@chugai-pharm.co.jp)
†These authors contributed equally to this work.

In this study, we histopathologically compared SC models and ORT models of a cell line that originated from adenocarcinoma of the gastroesophageal junction, OE19. Then we applied CASTIN to investigate the difference in cancer-stroma interactions.

Materials and Methods

Cell culture

OE19[17], a cell line of adenocarcinoma from the gastric cardia/esophageal gastric junction, was purchased from the European Collection of Authenticated Cell Cultures (ECACC No. 96071721). The cells were maintained in RPMI 1640 (Merck, Darmstadt, Germany) supplemented with 10% FBS, 10 mM HEPES, 1 mM sodium pyruvate, and 2.5 g/L glucose and cultured at 37°C in a 5% CO_2 incubator.

Animals

Six-week-old male C.B-17/lcr-scid/scid Jcl severe combined immune-deficient (SCID) mice were provided by CLEA Japan, Inc. (Tokyo, Japan). All animals were housed in a specific pathogen-free environment under controlled conditions (temperature, 20–26°C; humidity, 30–70%; light/dark cycle, 12/12 h) and were allowed to acclimatize and recover from shipping-related stress for more than 7 days prior to the study. Chlorinated water and irradiated food were provided *ad libitum*. The health of the mice was monitored by daily observation. All animal experiments were performed at Chugai Pharmaceutical Co., Ltd. The experiments were reviewed and approved by the Institutional Animal Care and Use Committee at Chugai Pharmaceutical Co., Ltd.

Xenograft models

For the SC implantation model, 1×10^5 cells were suspended in 200 µL of RPMI 1640 medium containing 50% Matrigel (Corning, NY, USA) and injected subcutaneously into the right flank of mice. For the ORT implantation model, the mice were inoculated with 1×10^5 cells suspended in 20 µL of RPMI-1640 medium containing 50% Matrigel. A surgical incision was made in the abdomen under isoflurane anesthesia, and the cells were inoculated under the serosal membrane of the ventral stomach wall. The tumors were sampled at 3 weeks after inoculation. For the ORT model, an additional time point was set at 6 weeks. For the SC model, no additional time points were set because there was notable necrosis in the center of the tumor after 4 weeks. At necropsy the animals were sacrificed under isoflurane inhalation anesthesia by exsanguination from the abdominal artery and grossly examined.

Tumor tissue sampling

ORT transplantation is not always successful, so it is necessary to select the cases that are appropriate for analysis. For the current study, 4 cases each were selected for both time points. Two cases were subjected to histopathology, and 2 cases were subjected to RNA analysis. For SC transplantation, 2 cases were used for histopathological examination, and 3 cases were used for RNA analysis.

Histopathological analysis

The tumor tissues were fixed in 10% neutral buffered formalin for 24 h and embedded into paraffin by a routine method. The tissues were sectioned at a thickness of 3–4 µm, and each tissue was subjected to hematoxylin and eosin and Masson's trichrome staining. The slides were examined under light microscopy.

Transcriptome sequencing

Tumors were embedded in O.C.T. compound (Sakura Finetek, Japan) and frozen in liquid nitrogen. Cryosections were prepared and suspended in TRIzol reagent (Thermo Fisher Scientific, Waltham, MA, USA), and total RNA was extracted according to the manufacturer's instructions. One microgram of total RNA was used to prepare a transcriptome sequencing library for each tumor sample using a TruSeq stranded mRNA Library Prep Kit (Illumina, San Diego, California, USA) according to the manufacturer's directions. The libraries were sequenced in 100 bp paired-end reads on a HiSeq 2500 sequencer (Illumina). Four libraries were loaded into the single lane of an Illumina flow cell, producing more than 30 million paired-end reads for each sample. Sequenced reads were then mapped to all RefSeq transcripts of the human (hg38 coordinates) and mouse (mm10 coordinates) using Bowtie 1.1.2, allowing up to one mismatch, and reads mapped to both species or to multiple genes were discarded. The remaining reads were used to estimate the gene expression profile of human cancer cells and mouse stroma cells according to the methods in our previous report[14].

Analysis of transcriptomic data

For unsupervised hierarchical clustering analysis, a Euclidean distance calculation and Ward's linkage were performed for the 500 most variable genes, defined by the coefficient of variation calculated across all samples using the Strand NGS software (ver. 2.6, Agilent Technologies, Santa Clara, CA, USA). Differentially expressed genes (DEGs) between SC and ORT models were selected using an empirical criterion of more than 3-fold change. To gain an overview of gene pathway networks, KEGG (Kyoto Encyclopedia of Genes and Genomes) analysis was performed using an online KEGG automatic annotation server (https://david.ncifcrf.gov/summary.jsp). The KEGG pathways identified were ranked by P-value.

CASTIN analysis

Interactome profiles were visualized by a modified version of the original CASTIN[14]. In the modified version, cancer ligand dependency X and stromal receptor dependency Y for each interaction were calculated as follows:

$$X = \frac{L_C}{L_C + L_S},$$

$$Y = \frac{R_S}{R_C + R_S},$$

where, L_C, L_S, R_C, and R_S, are normalized gene expression levels of ligand gene of human (cancer), ligand gene of mouse (stroma), receptor gene of human (cancer), and receptor gene of mouse (stroma), respectively. The signal strength of ligand H and receptor V were calculated as follows:

$$H = \ln(\max_{k\in\{C,S\}} L_k),$$

$$V = \ln(\max_{k\in\{C,S\}} R_k).$$

These four interactome evaluation indices (X, Y, H, V) were visualized for each interaction as a rhombus in the 2D-plane at position (X, Y), and the horizontal and vertical diagonal lengths were proportional to H and V, respectively. Then each interaction falls into one of the following four zones. 1) C-S zone (X≥0.5 and Y≥0.5): interactions in this zone indicate that input signals are dominantly created by cancer and exclusively transmitted to stroma. Signal transduction takes place only when both cancer and stromal cells exist, and thus we call it a "mutually dependent interaction." 2) S-C zone (X<0.5 and Y<0.5): interactions in this zone also indicate mutually dependent interactions, but the direction of signal transduction is opposite (stroma to cancer). 3) C-C zone (X≥0.5 and Y<0.5): input signals are created by cancer and transmitted mainly to cancer itself. Thus interactions in this zone indicate cancer autoregulation. 4) S-S zone (X<0.5 and Y≥0.5): a counterpart to the C-C zone. Interactions in this zone indicate microenvironment autoregulation.

Results and Discussion

Necropsy was performed in the SC and ORT models of OE19. In SC models, tumor formation was confirmed in all animals. In ORT models at 3 weeks, tumor formation at the inoculation site in the stomach was observed (Table 1). At 6 weeks, in addition to the changes at the inoculation site, there was infiltration of the tumors into other areas of the stomach and also metastasis in the pancreaticoduodenal lymph nodes, which shows that the area of tumor growth had expanded compared with that at 3 weeks (Table 1).

Next the area of inoculation was examined histopathologically in SC models at 3 weeks and ORT models at 3 and 6 weeks. With SC models, the SC mass was relatively well circumscribed from the surrounding tissue, and tumor growth was mainly expansive. The tumor cells formed large ductal structures with scant stroma (Fig. 1A). The ductal wall was relatively thick, and the tumor cells were often multilayered (Fig. 1B). With the ORT models, there was also tumor formation in the inoculation area, but the tumor cells formed smaller ducts that invaded into abundant stroma, and the growth was mainly invasive (Fig. 1A). The ductal wall consisted of a single layer of tumor cells (Fig. 1B). At 6 weeks in the ORT model, the monolayered small ducts were more densely packed, with less stroma than at 3 weeks (Fig. 1A and B). Vascular invasion was noted in the surrounding tissues (Fig. 2). Thus, there was a striking difference in growth patterns and the amount of stromal tissues between the 2 models. Notably, the invasive growth in the ORT model was thought to show that there was active interaction between the tumor and stromal cells, so the OE19 ORT model was thought to be suitable for analysis of cancer-stroma interactions. There is little information concerning the difference in the amount of stroma between SC and ORT models, but we speculate that this finding is at least common among some tumors, because similar results have been described in a xenograft model of pancreatic cancer[18]. Additional studies are considered necessary to further elucidate this matter.

In order to analyze the interactions between cancer cells and their microenvironment, we performed RNA sequencing of each xenograft model and simultaneously obtained OE19 (human) and stroma (mouse) transcriptome data. Before CASTIN analysis, we compared the gene expression profiles of OE19 cells between SC models and ORT models. Unsupervised hierarchical clustering showed that the expression profiles of SC-SC and ORT-ORT samples were consistent and clustered together into distinct groups (Fig. 3B). The difference in expression pattern between SC and ORT models at 3 weeks is represented in the scatter plot in Fig. 3C, for which differentially expressed genes (DEGs) were chosen using an empirical criterion of more than 3-fold change. Seventy-seven genes were highly expressed in SC models, and 168 genes were highly expressed in ORT models. To identify activated pathways in each model, DEGs were subjected to KEGG pathway enrichment analysis. The significant pathways with the highest representation are shown in Table 2. In the SC models, we could not find sig-

Table 1. Extent of Nodule Formation and Infiltration of Tumor

Findings	Weeks after inoculation	
	3	6
Tumor, stomach		
Inoculation site	4	4
Infiltration, other areas*	0	4
Tumor, other organs		
Pancreaticoduodenal lymph node	0	2

There were 4 animals for each timepoint. Numbers indicate the number of animals with findings. *Other areas include the small curvature and dorsal side of the stomach.

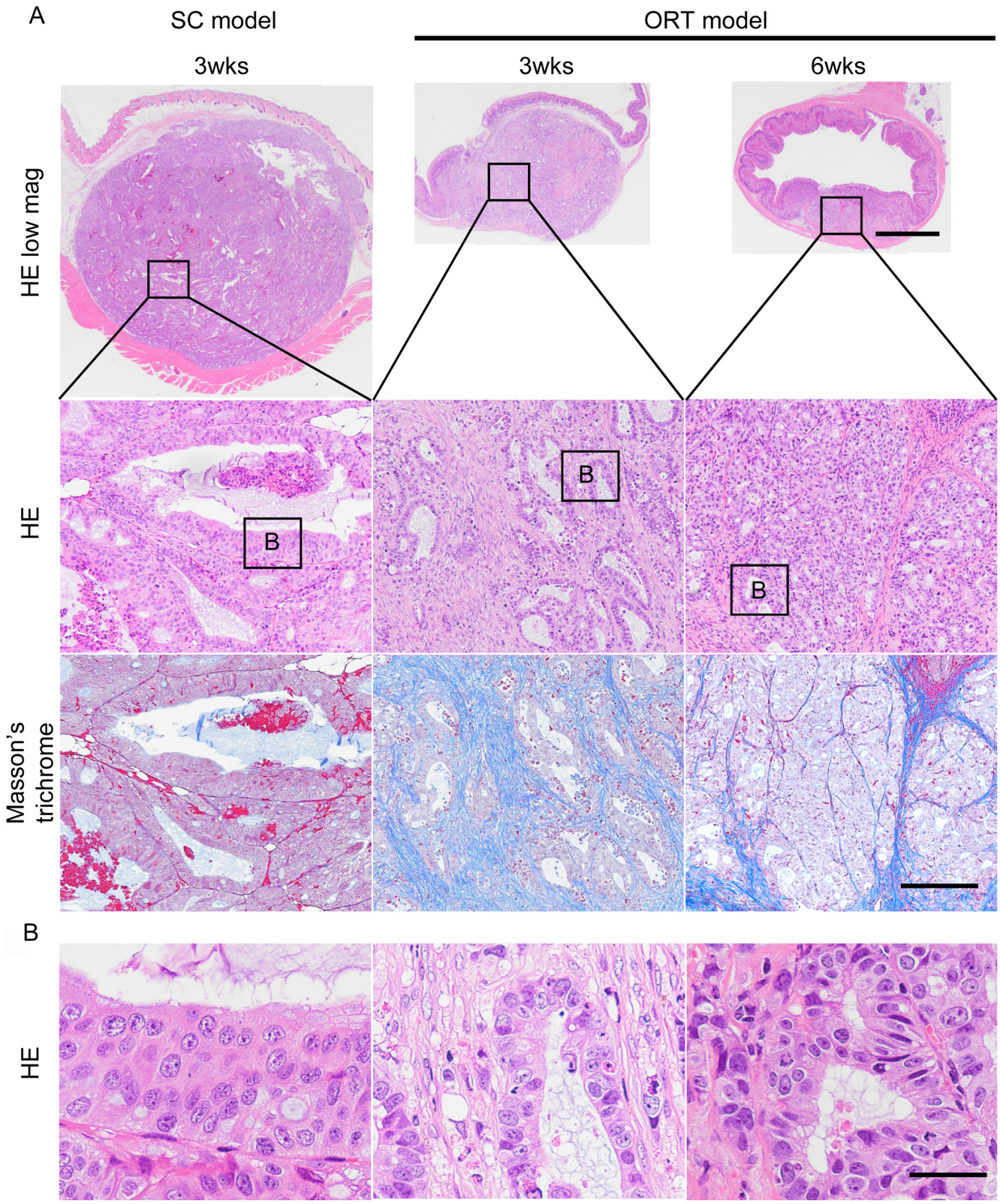

Fig. 1. Morphological comparison of SC and ORT inoculation of OE19. (A) At low magnitude, bar = 4,000 μm; in others, bar = 500 μm. (B) Bar = 100 μm.

nificantly enhanced pathways, but in the ORT models, we found that several signaling pathways including MAPK signaling, focal adhesion, and ECM-receptor interaction were enhanced. These data confirm that the OE19 status in SC and ORT models is different not only at the transcriptome level but also in the pathological analysis described above.

To understand the difference in cancer-stroma interaction between SC and ORT models, we applied CASTIN to the data set of each model. Interactome profiles of SC and ORT models at 3 weeks were visualized in Fig. 3D. Each data point on the plot represents an individual interaction, and the positions indicate the role of the interaction in cancer-stroma relationships. Interactions that direct a cancer ligand to a stromal receptor were plotted in the upper right zone (C-S zone), and those that direct a stromal ligand to a cancer receptor were plotted in the bottom left zone (S-C zone). Many interactions were plotted in the C-S zone and S-C zone for both SC and ORT models. To focus on interactions that were selectively enhanced in each model, we chose ligands or receptors that were included in the DEGs designated by the OE19 expression profiles (shown in dark colors in the CASTIN plots). In the SC model, 10 ligands or receptors included in the DEGs of the OE19 expression profiles were chosen, but none of their interactions were plotted in the C-S zone or S-C zone. On the other hand, in the ORT model, 44 ligands or receptors included in the DEGs of the OE19 expression profiles were chosen, and the interactions GAST-CCKBR, EDN1-EDNRB, CXCL3-CXCR2, CYR61-ITGB3, and DKK1-LRP6 were plotted in the C-S zone, so these interactions were thought to affect connections from cancer to stromal cells. The interaction TNFSF12-TNFRSF12A was plotted in the S-C zone and was therefore thought to affect connections from stromal to cancer cells. The ligand/receptor expression of OE19 cells in each model are compared in Fig. 3E. Interestingly, most interactions detected in this study were well known to affect tumor migration or the microenvironment[19–25]. These results indicate that CASTIN analysis could successfully identify several cancer-stroma interactions that may affect invasive growth of OE19 cells observed in the ORT model.

CASTIN provides a comprehensive view of cancer-stromal interactions and is useful to identify critical interactions in xenograft models. In this system, the expression profiles of stromal cells are obtained from whole mouse cells surrounding the xenograft tumors. Because the composition of mouse cells varied greatly between SC and ORT models in this study, it was difficult to choose interactions that affect the tumor microenvironment. By focusing on DEGs, we successfully identified several interactions that were selectively enhanced in ORT models. Even so, the accuracy of CASTIN analysis would be maximized by combining transcriptional information of cancer and stromal cells, so now we plan to use CASTIN to analyze against gene-modified cells (overexpression or knockdown) that have been inoculated at the same site to understand the molecular function of genes in a heterogeneous cancer microenvironment.

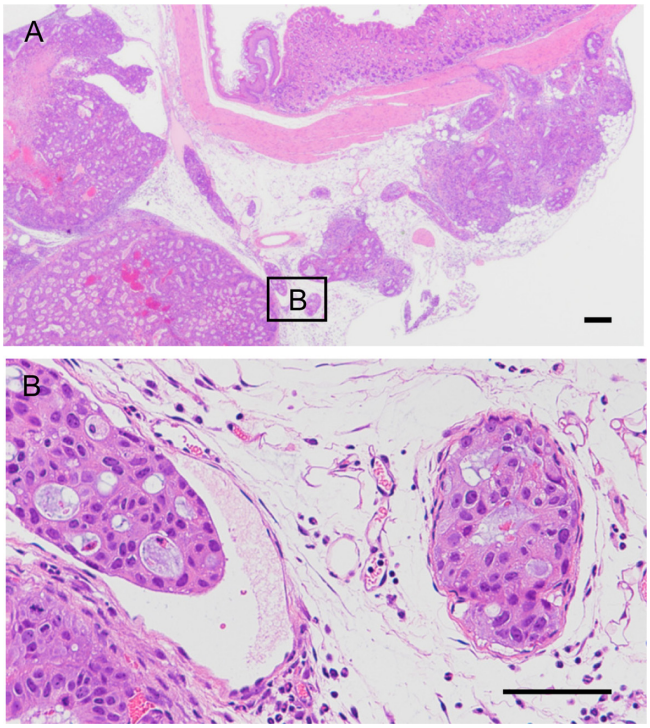

Fig. 2. Vascular invasion of OE19 cells. Hematoxylin and eosin stain. Bar = (A) 500 µm, (B) 200 µm.

Table 2. Upregulated Pathways in the ORT Model

KEGG ID	Term	P-value	Genes
hsa04010	MAPK signaling pathway	7.52×10^{-7}	FGF19, PDGFA, CACNG4, NR4A1, HSPA1A, FLNA, DUSP5, DUSP1, JUN, HSPA6, HSPB1, RRAS, PLA2G4C, GADD45B, DUSP8
hsa04510	Focal adhesion	2.75×10^{-6}	CAV2, CAV1, LAMA3, FYN, PDGFA, JUN, TNC, COL6A1, THBS1, COL11A2, BIRC3, FLNA, MYL9
hsa05134	Legionellosis	2.86×10^{-5}	CXCL1, CXCL3, CXCL2, HSPA6, CXCL8, TLR4, HSPA1A
hsa04668	TNF signaling pathway	1.77×10^{-4}	CXCL1, CCL20, CXCL3, JUN, EDN1, CXCL2, CX3CL1, BIRC3
hsa05132	Salmonella infection	3.22×10^{-4}	CXCL1, CXCL3, JUN, CXCL2, CXCL8, TLR4, FLNA
hsa05205	Proteoglycans in cancer	1.77×10^{-3}	CAV2, CAV1, HSPG2, RRAS, TLR4, WNT11, MSN, THBS1, FLNA
hsa04512	ECM-receptor interaction	2.89×10^{-3}	LAMA3, TNC, HSPG2, COL6A1, THBS1, COL11A2
hsa04115	p53 signaling pathway	6.73×10^{-3}	BBC3, SERPINE1, SFN, THBS1, GADD45B
hsa04390	Hippo signaling pathway	6.95×10^{-3}	BMP2, CTGF, BBC3, SERPINE1, WNT11, AREG, LATS2

KEGG, Kyoto Encyclopedia of Genes and Genomes.

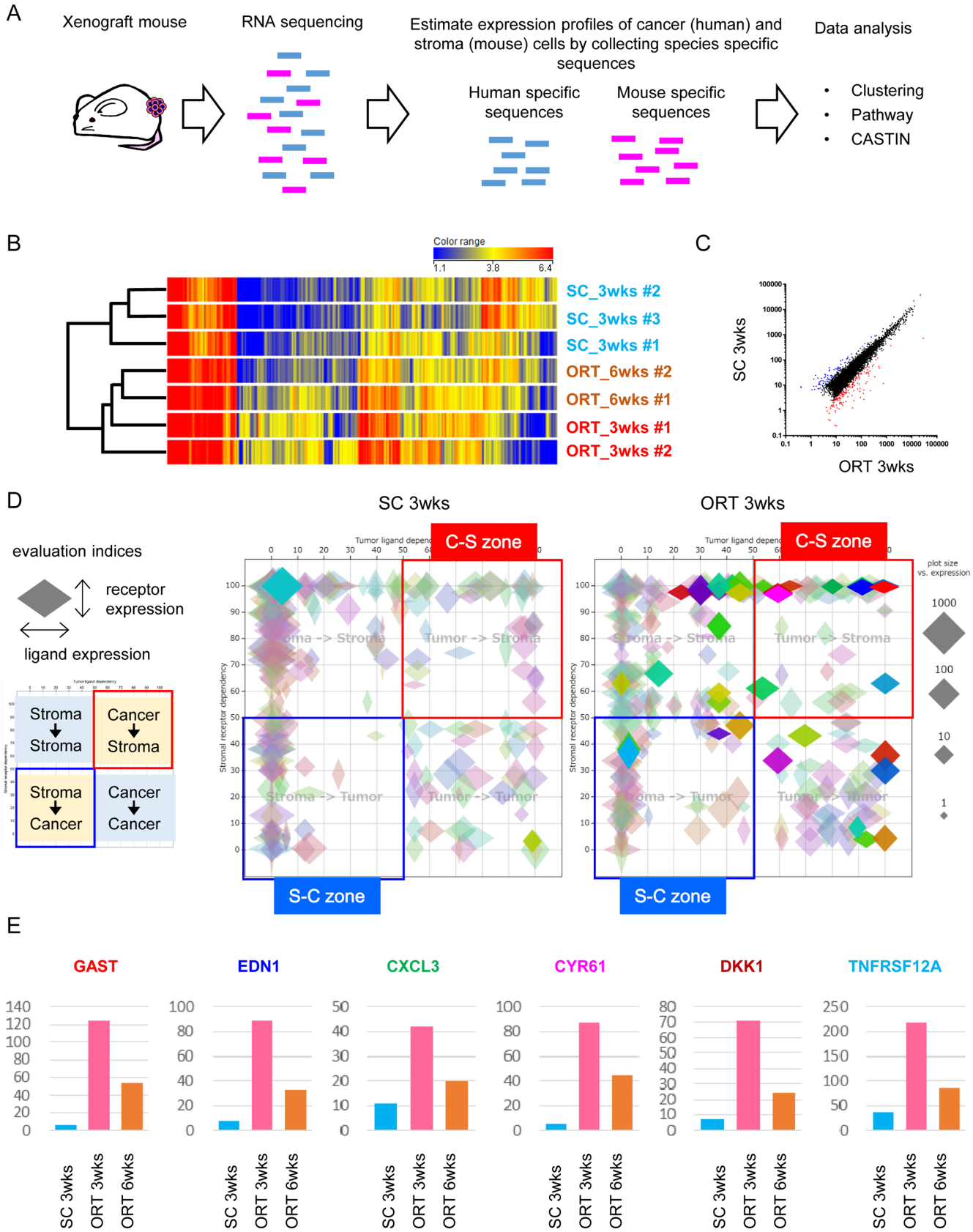
A
Xenograft mouse
RNA sequencing
Estimate expression profiles of cancer (human) and stroma (mouse) cells by collecting species specific sequences
Human specific sequences
Mouse specific sequences
Data analysis
Clustering
Pathway
CASTIN
B
Color range
1.1
3.8
6.4
SC_3wks #2
SC_3wks #3
SC_3wks #1
ORT_6wks #2
ORT_6wks #1
ORT_3wks #1
ORT_3wks #2
C
SC 3wks
ORT 3wks
D
evaluation indices
receptor expression
ligand expression
Stroma Stroma
Cancer Stroma
Stroma Cancer
Cancer Cancer
SC 3wks
ORT 3wks
C-S zone
S-C zone
Stromal receptor dependency
plot size vs. expression
1000
100
10
1
E
GAST
EDN1
CXCL3
CYR61
DKK1
TNFRSF12A
SC 3wks
ORT 3wks
ORT 6wks

Fig. 3.

Fig. 3. Interactome profiling of SC and ORT models. (A) Schematic workflow to estimate species-specific RNA expression profiles. (B) Hierarchical clustering of the differentially expressed genes across all samples. (C) Differentially expressed genes in SC and ORT at 3 weeks are plotted in a scatter plot. The values of the X and Y axes are the averaged normalized values in each group. Red dots indicate highly expressed genes with a fold change > 3 in the ORT model. Blue dots indicate highly expressed genes with a fold change > 3 in the SC model. (D) Interactome profiles of SC and ORT models at 3 weeks. Each data point represents an individual interaction. The size of the plot indicates the level of ligand or receptor expression. Interactions that connect a cancer ligand to a stromal receptor are plotted in the C-S zone (shown in red), while those that connect a stromal ligand to a cancer receptor are plotted in the S-C zone (shown in blue). (E) A comparison of the ligand/receptor expression of OE19. The corresponding interactions in each plot are shown in the same color.

Disclosure of Potential Conflicts of Interest: There are no conflicts of interest related to this study.

Acknowledgments: We would like to thank Ms. C. Ishimaru, Ms. M. Kinoshita, and Ms. Y. Kuroiwa of Chugai Research Institute for Medical Science Co., Ltd., and Dr. T. Ito of Chugai Phramaceutical Co., Ltd., for conducting the *in vivo* experiments and Ms. Y. Ohtani of Chugai Research Institute for Medical Science for preparing the histopathological slides.

References

1. Bibby MC. Orthotopic models of cancer for preclinical drug evaluation: advantages and disadvantages. Eur J Cancer. **40**: 852–857. 2004. [Medline] [CrossRef]
2. Loi M, Di Paolo D, Becherini P, Zorzoli A, Perri P, Carosio R, Cilli M, Ribatti D, Brignole C, Pagnan G, Ponzoni M, and Pastorino F. The use of the orthotopic model to validate antivascular therapies for cancer. Int J Dev Biol. **55**: 547–555. 2011. [Medline] [CrossRef]
3. Zhan B, Wen S, Lu J, Shen G, Lin X, Feng J, and Huang H. Identification and causes of metabonomic difference between orthotopic and subcutaneous xenograft of pancreatic cancer. Oncotarget. **8**: 61264–61281. 2017. [Medline] [CrossRef]
4. Hiroshima Y, Zhang Y, Zhang N, Uehara F, Maawy A, Murakami T, Mii S, Yamamoto M, Miwa S, Yano S, Momiyama M, Mori R, Matsuyama R, Chishima T, Tanaka K, Ichikawa Y, Bouvet M, Endo I, and Hoffman RM. Patient-derived orthotopic xenograft (PDOX) nude mouse model of soft-tissue sarcoma more closely mimics the patient behavior in contrast to the subcutaneous ectopic model. Anticancer Res. **35**: 697–701. 2015. [Medline]
5. Killion JJ, Radinsky R, and Fidler IJ. Orthotopic models are necessary to predict therapy of transplantable tumors in mice. Cancer Metastasis Rev. **17**: 279–284. 1998-1999. [Medline] [CrossRef]
6. Igarashi K, Kawaguchi K, Kiyuna T, Murakami T, Miwa S, Nelson SD, Dry SM, Li Y, Singh A, Kimura H, Hayashi K, Yamamoto N, Tsuchiya H, Eilber FC, and Hoffman RM. Patient-derived orthotopic xenograft (PDOX) mouse model of adult rhabdomyosarcoma invades and recurs after resection in contrast to the subcutaneous ectopic model. Cell Cycle. **16**: 91–94. 2017. [Medline] [CrossRef]
7. Dai L, Lu C, Yu XI, Dai LJ, and Zhou JX. Construction of orthotopic xenograft mouse models for human pancreatic cancer. Exp Ther Med. **10**: 1033–1038. 2015. [Medline] [CrossRef]
8. Du Q, Jiang L, Wang XQ, Pan W, She FF, and Chen YL. Establishment of and comparison between orthotopic xenograft and subcutaneous xenograft models of gallbladder carcinoma. Asian Pac J Cancer Prev. **15**: 3747–3752. 2014. [Medline] [CrossRef]
9. Zhang Y, Toneri M, Ma H, Yang Z, Bouvet M, Goto Y, Seki N, and Hoffman RM. Real-Time GFP Intravital Imaging of the Differences in Cellular and Angiogenic Behavior of Subcutaneous and Orthotopic Nude-Mouse Models of Human PC-3 Prostate Cancer. J Cell Biochem. **117**: 2546–2551. 2016. [Medline] [CrossRef]
10. Furukawa T, Kubota T, Watanabe M, Kitajima M, and Hoffman RM. Orthotopic transplantation of histologically intact clinical specimens of stomach cancer to nude mice: correlation of metastatic sites in mouse and individual patient donors. Int J Cancer. **53**: 608–612. 1993. [Medline] [CrossRef]
11. Fung AS, Lee C, Yu M, and Tannock IF. The effect of chemotherapeutic agents on tumor vasculature in subcutaneous and orthotopic human tumor xenografts. BMC Cancer. **15**: 112. 2015. [Medline] [CrossRef]
12. Song C, Hong BJ, Bok S, Lee CJ, Kim YE, Jeon SR, Wu HG, Lee YS, Cheon GJ, Paeng JC, Carlson DJ, Kim HJ, and Ahn GO. Real-time Tumor Oxygenation Changes After Single High-dose Radiation Therapy in Orthotopic and Subcutaneous Lung Cancer in Mice: Clinical Implication for Stereotactic Ablative Radiation Therapy Schedule Optimization. Int J Radiat Oncol Biol Phys. **95**: 1022–1031. 2016. [Medline] [CrossRef]
13. Fidler IJ, Wilmanns C, Staroselsky A, Radinsky R, Dong Z, and Fan D. Modulation of tumor cell response to chemotherapy by the organ environment. Cancer Metastasis Rev. **13**: 209–222. 1994. [Medline] [CrossRef]
14. Komura D, Isagawa T, Kishi K, Suzuki R, Sato R, Tanaka M, Katoh H, Yamamoto S, Tatsuno K, Fukayama M, Aburatani H, and Ishikawa S. CASTIN: a system for comprehensive analysis of cancer-stromal interactome. BMC Genomics. **17**: 899. 2016. [Medline] [CrossRef]
15. Makałowski W, Zhang J, and Boguski MS. Comparative analysis of 1196 orthologous mouse and human full-length mRNA and protein sequences. Genome Res. **6**: 846–857. 1996. [Medline] [CrossRef]
16. Bainer R, Frankenberger C, Rabe D, An G, Gilad Y, and Rosner MR. Gene expression in local stroma reflects breast tumor states and predicts patient outcome. Sci Rep. **6**: 39240. 2016. [Medline] [CrossRef]
17. Rockett JC, Larkin K, Darnton SJ, Morris AG, and Matthews HR. Five newly established oesophageal carcinoma cell lines: phenotypic and immunological characterization.

Br J Cancer. **75**: 258–263. 1997. [Medline] [CrossRef]
18. Hoover M, Adamian Y, Brown M, Maawy A, Chang A, Lee J, Gharibi A, Katz MH, Fleming J, Hoffman RM, Bouvet M, Doebler R, and Kelber JA. A novel method for RNA extraction from FFPE samples reveals significant differences in biomarker expression between orthotopic and subcutaneous pancreatic cancer patient-derived xenografts. Oncotarget. **8**: 5885–5894. 2017. [Medline] [CrossRef]
19. Smith JP, Nadella S, and Osborne N. Gastrin and Gastric Cancer. Cell Mol Gastroenterol Hepatol. **4**: 75–83. 2017. [Medline] [CrossRef]
20. Rosanò L, Spinella F, and Bagnato A. Endothelin 1 in cancer: biological implications and therapeutic opportunities. Nat Rev Cancer. **13**: 637–651. 2013. [Medline] [CrossRef]
21. See AL, Chong PK, Lu SY, and Lim YP. CXCL3 is a potential target for breast cancer metastasis. Curr Cancer Drug Targets. **14**: 294–309. 2014. [Medline] [CrossRef]
22. Wells JE, Howlett M, Cole CH, and Kees UR. Deregulated expression of connective tissue growth factor (CTGF/CCN2) is linked to poor outcome in human cancer. Int J Cancer. **137**: 504–511. 2015. [Medline] [CrossRef]
23. Li J, Ye L, Owen S, Weeks HP, Zhang Z, and Jiang WG. Emerging role of CCN family proteins in tumorigenesis and cancer metastasis (Review) (Review). Int J Mol Med. **36**: 1451–1463. 2015. [Medline] [CrossRef]
24. Zhuang X, Zhang H, Li X, Li X, Cong M, Peng F, Yu J, Zhang X, Yang Q, and Hu G. Differential effects on lung and bone metastasis of breast cancer by Wnt signalling inhibitor DKK1. Nat Cell Biol. **19**: 1274–1285. 2017. [Medline] [CrossRef]
25. Hu G, Zeng W, and Xia Y. TWEAK/Fn14 signaling in tumors. Tumour Biol. **39**: 1010428317714624. 2017. [Medline] [CrossRef]